CrossMark

Basic red 2 and methyl violet adsorption by date pits: adsorbent characterization, optimization by RSM and CCD, equilibrium and kinetic studies

Manel Wakkel[1] · Besma Khiari[1] · Féthi Zagrouba[1]

Abstract

The potential of raw date pits as a natural, widely available and low-cost agricultural waste has been studied in order to adsorb cationic dyes from an aqueous solution. Date pits were characterized by FTIR, SEM, BET, and XRD analysis. To optimize removal of two industrial dyes, basic red 2 (BR2) and methyl violet (MV), from aqueous solution using date pits, response surface methodology (RSM) is employed. Tests were carried out as per central composite design (CCD) with four input parameters namely contact time, temperature, initial concentration of adsorbate, and pH. Second-order polynomial model better fits experimental data for BR2 and MV and optimum values were then determined. In the optimum conditions, kinetic study was conducted and the pseudo-second-order model was found the best fitted model compared to pseudo-first-order model. Moreover, it was shown that intraparticle diffusion was not the sole controlling step and could be associated with other transfer resistance. On other hand, equilibrium isotherms were obtained for BR2 and MV and their maximum adsorption capacities were 92 and 136 mg g^{-1} respectively. Two-parameter isotherm models like Langmuir, Temkin, Freundlich, Dubinin–Radushkevich, and Halsay were investigated to fit equilibrium data. Three error functions of residual root mean square error, chi-square statistic, and average relative error were used to comfort us in the selected models, which were actually Dubinin–Radushkevich and Langmuir for BR2 and Frendlich, Temkin, and Halsay for MV.

Keywords Adsorption · Basic red 2 · Methyl violet · Date pits · Equilibrium isotherm · Response surface methodology

Introduction

Synthetic dyes represent one of the major water contaminants in industry (Adegoke and Bello 2015). More than 7×10^5 tons of dyes are produced worldwide annually (Ayhan 2009; Ibrahim et al. 2010; Raval et al. 2016). About 12% of produced synthetic dyes are lost during manufacturing and processing operations (Hashem et al. 2007; Hema and Arivoli 2007). Textile, food, and paper industries generate considerable amounts of colored wastewaters which are toxic and even carcinogenic and mutagenic (Das et al. 2015; Ardejani et al. 2007).

Several physical, chemical, and biological techniques were applied to the treatment of wastewater (Ferrero 2007). Among all these methods, adsorption is one of the most attractive techniques owing to its simplicity, flexibility, cost, and suitability for batch and continuous processes (Kesraoui et al. 2017; Limousy et al. 2017; Miraboutalebi et al. 2017; Rozumová et al. 2016; Muthanna 2016).

Low cost, quite abundance, and renewability of agricultural biomass make them promising adsorbent for large variety of pollutants (Muthanna 2016; Amor and Ismail 2015; Ahmed and Theydan 2014; Briones et al. 2011; El-Naas et al. 2010). One can cite orange peel (Emanuele Lessa et al. 2017), date pits (Muthanna 2016), cashew nut shell (Subramaniam and Ponnusamy 2015), olive pomace (Banat et al. 2007), and almond peel (Benaissa 2010). In Tunisia, date production has moved from 103,000 to 225,000 tons between 2000 and 2015 (interprofessional grouping of fruits 2015). Yet, apart from its use as animal feedstock or its transformation into bioethanol

---

Responsible editor: Guilherme L. Dotto

✉ Besma Khiari
    besmakhiari@yahoo.com

[1] Research Laboratory of Environmental Science and Technologies,
    Borj Cédria, 2050 Hammam-Lif, Tunisia

or biomethane in few small units, no other recovery method is applied in the Tunisian context.

In adsorption process, the chemistry of the sorbent surface is as important as its textural properties particularly when the sorption process involves electrostatic interaction between the solute molecules and some active sites on the sorbent available surface. Thus, determining pore size, surface area, and functional groups allows to explain the possible mechanisms of dyestuff removal from multiphase or homogenous systems by adsorption process (Ashour 2010).

In order to ensure an efficient removal of pollutants from water and to maximize the adsorption yield, an optimization study should be conducted (Garbaa et al. 2015). The improvement and the optimization of the processes can be carried out by response surface methodology (RSM) which is defined as a combination between mathematical and statistical approaches (Wang 2013). In fact, RSM can be considered as an efficient tool to study the effect of process variables in the defined response as well as the interactions between all the factors (Das et al. 2015). The strong point of this tool in process optimization is to lower the experiment number and thus the time and the cost of the adsorption process (Lee et al. 2000; Alam et al. 2007).

The novelty of this work consists in using date pits as an adsorbent of two basic dyes, namely basic red 2 and methyl violet, which never underwent adsorption operation by this agro-industrial waste. In fact, according to the literature, BR2 and MV were removed by some other adsorbents such as soybean hull (Chandane and Sing 2014), local clay (Miyah et al. 2017), and soil composites (Das et al. 2015). At the same time, date stones were reported as efficient adsorbent materials to remove several dyes such as methylene blue and methyl orange (Mahmoudi et al. 2015). But to our knowledge, the combinations (date pits, BR2 and date pits, MV) were never tested. Our interest toward these two dyes is justified by their extensive and wide use in different industrial applications (textile, paper...) (Aljeboree et al. 2017) and their mitotic and mutagen effect on aquatic life (Körbahti and Rauf 2008).

Thus, the main objective of the present work is to examine the effectiveness of date pits for the removal of BR2 and MV from aqueous solution on batch system. Firstly, textural and chemical properties of date pits particles were described by the use of scanning electron microscopy, BET analysis, X-ray diffraction, and FTIR analysis. Secondly, sensitive operating parameters such as temperature, contact time, pH, and initial dye concentration have been tested. A central composite design (CCD) helped to determine the major factors and the mathematical model that predict the response as function of factor variations. Then, the optimum conditions were determined using the model and its relative response surfaces. Equilibrium isotherms and kinetics were determined using different models, the fitting of which was consolidated by three error functions.

Material and methods

Adsorbate

Basic red 2 (BR2), 3,7-diamino-2,8-dimethyl-5-phenylphenazinium chloride, and methyl violet (MV), hexamethylpararosaniline chloride, were supplied by Sigma-Aldrich, USA. Chemical structures of RB2 and MV are shown in Fig. 1 and their chemical properties are summarized in Table 1.

Dye stock solutions were prepared by dissolving 1 g of dye in 1 L distilled water and the desired dye concentrations were obtained by the dilution of the stock solution. Sodium hydroxide and hydrochloric acid solutions were used to adjust the pH.

Adsorbent

The date pits were collected from a date transformation industry located in Tunisia. After being washed by distilled water, the collected materials spent 24 h in an oven at 40 °C. Grinding and sieving steps followed to obtain particle sizes ranging from 125 to 250 μm. The final product was stored in an air-tight container.

Adsorbent characterization

The nitrogen adsorption/desorption isotherm was carried out to calculate the BET specific surface area (S_{BET}) of the date pits. To achieve these calculations, the sample was degassed at 120 °C for 4 h. BET analysis was carried out by N2-physisorption at 77 K using the surface area analyzer model Autosorb-1C (Quantachrome, USA) and the equation is applied on the adsorption isotherm for P/P_0 ranging from 0.05 to 0.35.

The surface texture of date pits was studied by a FEI QUANTA 200 scanning electron microscope (SEM). The substrate was placed on the aluminum tube, coated with gold for electron reflection, and vacuumed during 5 to 10 min.

For the purpose of analyzing the functional groups of date pits, a Fourier transform infrared spectroscopy (FTIR) analysis using potassium bromide (KBr, Merck) disks has been performed (Miraboutalebi et al. 2017). An amount of 1.5 mg of the dried substance were mixed with 250 mg KBr in agate mortar and the obtained mixture was pressed at 10 atm during 10 min. The FTIR spectra of the prepared disks were collected using a Perkin-Elmer Spectrum 2000 FTIR spectrometer. Recording was set from 4000 to 400 cm^{-1}.

The X-ray diffraction (XRD) analysis was conducted to study the crystallographic structure of date pits. A mass of 0.5 g of finely ground fruit stones is placed between the blade and the slide and introduced into the diffractometer. X-ray powder diffraction data were obtained on PHILIPS PW 3040

Fig. 1 Chemical structure of **a** basic red 2 and **b** methyl violet dyes

(a)

(b)
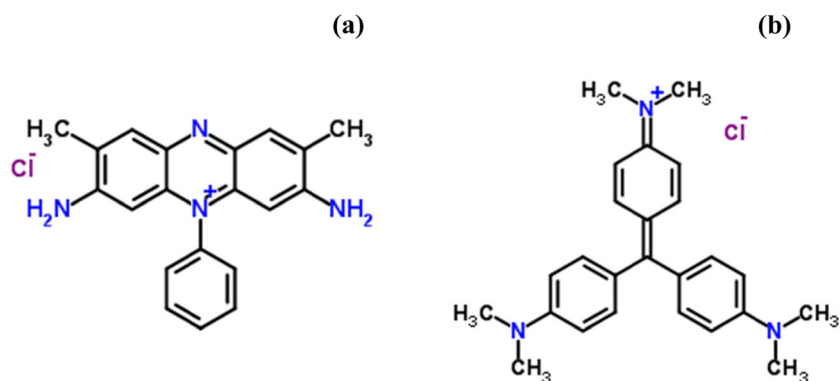
diffractometer. The wavelength of X-radiation was adjusted to 1.789 A° and scanning was done between $0° < 2\theta < 80°$.

The electrical neutrality of the date pits adsorbent can be specified by the point of zero charge (pH_{pzc}) at a value of pH under solution conditions (Saleh 2015). A batch equilibrium technique was carried out to determine the (pH_{pzc}) (Banat et al. 2007): 50 mL of NaCl solution (0.01 M) were placed in Erlenmeyer flasks. HCl (1 N) and NaOH (1 N) solutions were used to adjust the pH of NaCl solution between 2 and 12. The final pH was measured after adding 0.05 g of date pits and keeping solution under agitation during 6 h at room temperature (25 °C). The pH_{pzc} value was determined from the intersection of the curve [(pH_{final}) vs. ($pH_{initial}$)] and the bissector (Saleh 2015; Bohli et al. 2015).

Experimental design and analysis

CCD is a good tool to evaluate how far the response (percentages of BR2 and MV adsorption) is affected by independent variables and to optimize the relevant conditions in order to predict the best value of the response.

The four independent variables considered here are initial concentration (X_1), pH (X_2), temperature (X_3), and contact time (X_4). Based on some preliminary experiments (Table 2), these four variables undergo five different levels.

For a design of ($n = 4$) independent variables, total number (N) of experiments is given by (Lee et al. 2000; Myers and Montgomery 2001; Alam et al. 2007):

$$N = (2^n + 2n + n_c) = 30 \quad (1)$$

The range of each variable is firstly fixed, then a code is affected as follows:

   0: For the center points
   ±1: For factorial points
   ±α: For the axial points

where

$$\propto = \sqrt[4]{n} = 2 \quad (2)$$

The uncoded ith independent variable X_i is transformed into a dimensionless coded value x_i as (Zhu et al. 2016; Adinarayana and Ellaiah 2002):

$$x_i = \frac{(X_i - X_{i0})}{\Delta X_i} \quad (3)$$

where X_{i0} is the uncoded ith independent variable at the center point and ΔX_i is the step change value.

The coded and uncoded values corresponding to the four studied variables are summarized in Table 2.

The response variable named Y which is the percentage of adsorption by the date pits can be expressed as the following:

$$Y = f(X_1, X_2, X_3, ..., X_n) + e \quad (4)$$

In which, f is the response function and e is the experimental error (Singh[b] et al. 2012b).

A higher-order polynomial, such as quadratic model may express the predicted response Y as (Lee et al. 2000; Alam et al. 2007; Bhaumik and Mondal 2016):

$$Y = a0 \sum_{i=1}^{n} aiXi + \sum_{i=1}^{n} aii\, Xi2 + \sum_{i=1}^{n-1} \sum_{j=1}^{n} aij\, XiXj + e \quad (5)$$

where a_0, a_i, a_{ii}, and a_{ij} are, respectively, the constant, the linear, the quadratic, and the interaction coefficients.

The student's t test and the analysis of variance (ANOVA) were carried out to verify the signification of the regression coefficients and the adequacy of the selected model. Predicted and measured values of the response variable allowed us to calculate the correlation coefficient (R^2) (Lee et al. 2000; Alam et al. 2007; Garbaa et al. 2015).

The graphical and regression analysis as well as statistical significance were achieved using STAISTICA (trial version 9.0, StatSoft Inc., USA) software package to yield regression equations, regression coefficients, and analysis of variance (ANOVA). Contours were plotted to visualize the relationship between the variables and the response and to find an optimum parameters combination.

Table 1　Chemical properties of BR2 and MV

Properties	Basic red 2 (BR2)	Methyl violet (MV)
Chemical formula	$C_{20}H_{19}N_4Cl$	$C_{25}H_{30}N_3Cl$
Molecular weight (g/mol)	353	407
Wavelength (nm)	518	584
Solubility in water at 25 °C (g L^{-1})	50	16

Sorption procedure

Optimization, kinetic, and isotherm studies have been carried out to assess the adsorbent capacity and the sorption rate of basic red 2 and methyl violet removal from aqueous solution. In optimization study, adsorption tests were performed in 30 sets of 250-ml Erlenmeyer flasks filled with 100 mL of dye solution. Kinetic tests were performed at a fixed initial concentration of 60 mg/L for a period of time ranging from 5 to 240 min. In equilibrium study, different initial concentration (25–400 mg L^{-1}) were prepared and the adsorption reaction time was fixed to 120 min as this latter was proved to be long enough for the process to reach equilibrium according to kinetic results, on the one hand and according to some previous studies on the other hand.

Kinetic and equilibrium sorption tests were conducted according the same procedure. The pH of BR2 and MV solutions were fixed respectively on 7.7 and 7.28. A mass of 100 mg of date pits (size from 125 to 250 μm) was added to each flask and shaked at 125 rpm at 35 °C. After centrifugation (4000 rpm, 15 min), samples were taken from the solutions. The concentrations of basic red 2 and methyl violet in the supernatant liquids were determined using a double beam UV–vis spectrophotometer (UV-1601 Shimadzu, Japan) at their maximum wavelength of 518 and 584 nm, respectively.

The removal rate of BR2 and MV from the water was calculated using Eq. (6):

$$\text{Removal percentage} = \frac{(C0-Ce)}{C0} \times 100 \tag{6}$$

Table 2　Process control variables and their coded levels for the central composite design of dye adsorption

Variables	Code	Unit	Coded variable levels				
			$-\alpha$	-1	0	$+1$	$+\alpha$
Initial dye concentration	X_1	mg L^{-1}	25	50	75	100	125
pH	X_2	–	2	4	6	8	10
Temperature	X_3	°C	12.5	25	37.5	50	62.5
Contact tContact time	X_4	min	30	60	90	120	150

where C_o (mg L^{-1}) is the initial liquid-phase concentration of dye and C_e (mg L^{-1}) is the equilibrium liquid-phase concentration of dye.

At optimum conditions, the amount of the adsorbed dye q_t (mg g^{-1}) in t-time was calculated by the following mass balance equation:

$$q_t = \frac{(C_0-C_t)v}{w} \tag{7}$$

where v (L) is the volume of the solution, w (g) is the mass of dry sorbent and C_t (mg L^{-1}) is liquid-phase concentration of dye at any time t.

Moreover, the amount of dye uptake by the adsorbent at equilibrium, q_e (mg g^{-1}) was determined as follows:

$$q\text{e} = \frac{(C0-Ce)\cdot v}{w} \tag{8}$$

Results and discussions

Adsorbent characterization

Scanning electron microscopy analysis

As adsorption process is a surface phenomenon, it is mainly depending on the surface characteristics such as the number of pores present on the surface of the adsorbent material. The surface morphology and structure (textural and porous) of the adsorbent material was analyzed by scanning electron microscopy (SEM). SEM micrographs obtained at ×1000 and ×2000 magnification were shown in Fig. 2. SEM analysis revealed that date pits exhibited a rough surface with the presence of some macropores.

X-ray diffraction analysis

The powder X-ray diffraction of date pits data is shown in Fig. 3. The diffractogram did not exhibit a horizontal basic line and highlighted the presence of few diffraction peaks. This result indicates that the main structure of raw date pits is amorphous and its crystalline matter content is low.

BET analysis

The BET method was also carried out in order to determine the specific surface area (S_{BET}) of date pits particles, which was found 0.27 m^2 g^{-1}. Similarly to our results, Arami et al. (2006) showed low specific surface magnitude (0.76 m^2 g^{-1}) of the soy meal hull with high capacity of adsorption of direct red 80 (178.57 mg g^{-1}).

Fig. 2 SEM micrographs of date pits particles on **a** ×1000 and **b** ×2000 magnification
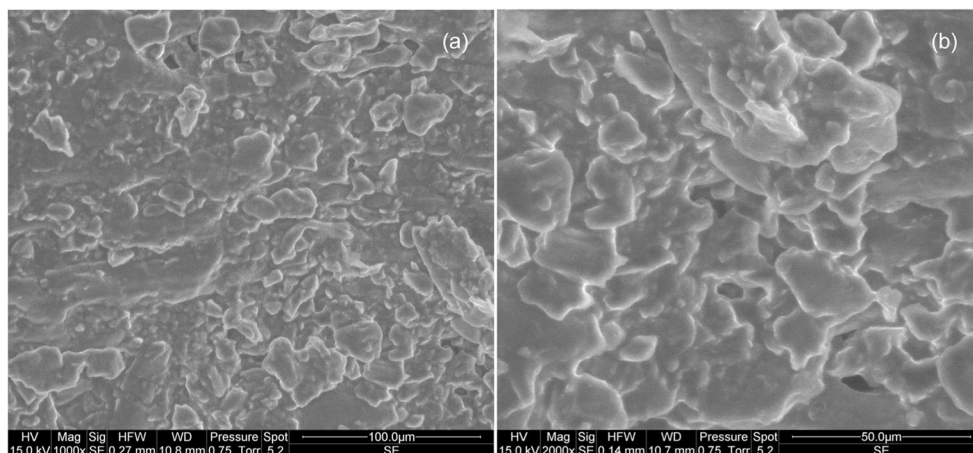
FTIR analysis

Since the adsorption capacity is strongly influenced by the surface chemistry of the adsorbent (Mane et al. 2007; Al-Ghouti et al. 2013), chemical structure is important to explore. Fourier transform infrared (FTIR) technique is an important tool to identify the characteristic functional groups and to study the interaction between an adsorbate and the active groups on the surface of the adsorbent.

The possible involvement of some functional groups of date pits was determined by using FTIR analysis. The FTIR spectrum has been analyzed by attenuated total reflectance within the range of 400–4000 cm^{-1} and was shown in Fig. 4.

As shown in the FTIR spectrum of date pits, a broad band of the O-H stretching vibration appears at 3396 cm^{-1}. It corresponds to both free and bonded hydroxyl groups (alcohols, phenols, and carboxylic acids) as in cellulose, pectin and lignin (Gnanasambandam and Protor 2000; Saeed et al. 2010).

Two adjacent bands located at 2922 and 2852 cm^{-1} can be attributed to C–H stretching of aldehyde molecules.

The band observed at 1745 cm^{-1} is the stretching vibration of C=O related to carbonyl groups (–COOH, –COOCH$_3$) and may be assigned to carboxylic acids or their esters (Farinella et al. 2007; Iqbal et al. 2009). The unconjugated C=O is abundant in xylans (hemicellulose). The band value at 1616 cm^{-1} relates to the bending mode of alkene group C=C.

The two bands observed at 1437 and 1375 cm^{-1} are attributed respectively to C-H deformation in lignin/carbohydrates and in cellulose/hemicellulose.

Adsorption band at 1240 cm^{-1} corresponds to the syringyl ring and C-O stretch in lignin and xylan. Bands located at 1156 and 1055 cm^{-1} are assigned respectively to C-O-C vibration and C-O stretch of alcoholic, ester, and carboxylic acids groups present in cellulose and hemicellulose (Al-Ghouti et al. 2013; Guibaud et al. 2003; Pandey and Pitman 2003).

Carbonyl and hydroxyl groups were also present in abundance which are essential for dye attraction from solution if the electrostatic mechanism is involved. Similarly to our results, it has been reported by Al-Ghouti et al. (2017) that the main functional groups in the raw date pits surface are

Fig. 3 X-ray diffraction patterns of raw date pits
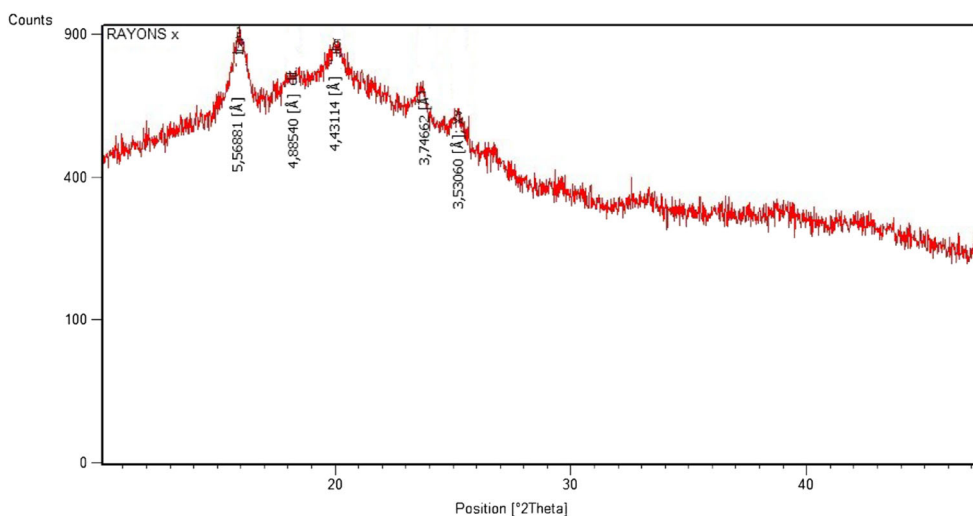
Fig. 4 FTIR spectra of raw date pits
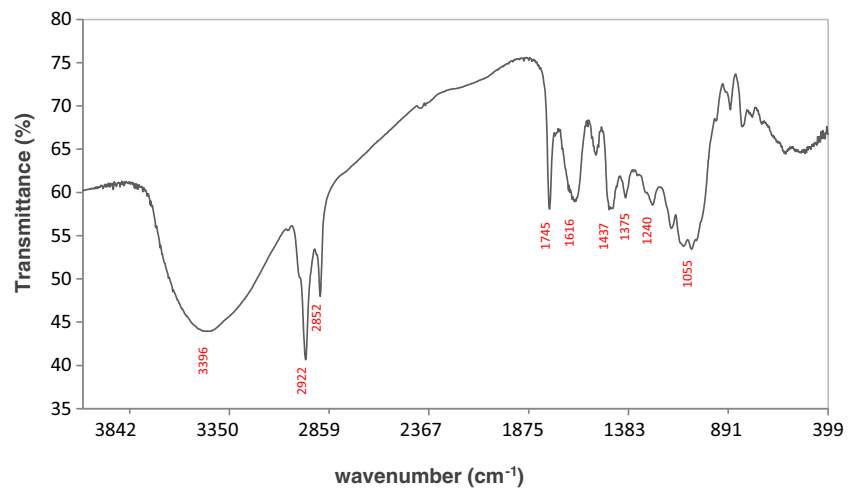
(alcohol O–H), (alkane C–H), (aldehyde, ketone, ester C=O), and (alcohol, ester C–O), contributing directly to the adsorption mechanisms.

pH$_{PZC}$ determination

Besides to FTIR analysis, the zero point of charge (pH$_{pzc}$) is an important parameter which characterize the chemistry of the adsorbent. The pH$_{PZC}$ is the point where positive and negative charges are equal on the substrate surface, which helps describing the properties of the resulting electrical double-layer interfaces. It determines the range of pH sensibility of an adsorbent and allows the prediction of the adsorbent charge in a specific pH solution (Guibaud et al. 2003; Saleh 2015).

The pH$_{pzc}$ of raw date pits was determined according to the procedure described above and was found equal to 6.8 (Fig. 5).

At pH values lower than 6.8, the adsorbent will have a net positive charge on the surface due to protonation (Saleh 2015). However, at pH values higher than 6.8, the surface has a net negative charge due to ionization since the amino groups of sorbent are deprotonated (Subramani and Thinakaran 2017). Thus, resulting attractive or repulsive forces depend on the pH$_{pzc}$ of the adsorbent, the pH of the solution, and on the nature of the adsorbate (anionic or cationic).

Response surface methodology

Central composite design was used to develop correlations (linear, quadratic, and interactive) between the four variables (X_1, X_2, X_3, X_4) and the response (Y). Thirty (30) runs of the CCD experimental design were conducted of which 6 runs were carried out at the center point to determine the experimental error "e." The complete design matrix of the batch experiments and the results obtained are shown in Table 3.

The observed percentage adsorption efficiencies varied from 20 to 94.36% for BR2 and from 18 to 96.13% for MV. Results indicated clearly that the BR2 and MV removal efficiencies were deadly sensitive to the selected variables in the present study.

Effects of model components on BR2 and MV removal efficiency

In order to study the variable effect on the dye adsorption, the values of the regressions coefficients were evaluated by STASTICA 9.0. Student's t test and p values were used to determine the significance of each regression coefficient. The larger is t and the smaller is p, the more significant is the corresponding parameter in the regression model (Yetilmezsoy and Saral 2007; Singh[a] et al. 2012a).

Regression coefficients, standard effects, standard errors (SE), t values, and probabilities of significance for the different model parameters were summarized in Table 4 for both dyes.

Results showed that for both dyes, the most influential components were the initial dye concentration X_1 ($t = -7.18$ for BR2; $t = -15.65$ for MV, $p = 0$) and initial pH of solution X_2 ($t = 28.85$ for BR2, $t = 38.05$ for MV, $p = 0$) since their t values are superior to the tabulated t value (2.776) for an error risk of 5%.

The quadratic terms of X_1^2 and X_2^2 were also considerably respectively important for BR2 ($t = -6.29$, $p = 0$ and $t = -18.08$, $p = 0$) and for MV ($t = -14.06$, $p = 0$ and $t = -31.47$, $p = 0$).

As seen in Table 4, the quadratic effects of the initial concentration of BR2 and MV (C_0, X_1^2) and the initial pH solution (pH, X_2^2) of BR2 and MV were found to be less significant than their respective linear effects (X_1 and X_2). However, the quadratic effect of temperature (X_3^2) was more significant than his first-order main (X_3) which shows the no-linear influence of the temperature on BR2 and MV adsorption.

Fig. 5 Date pits pH_{pzc} determination
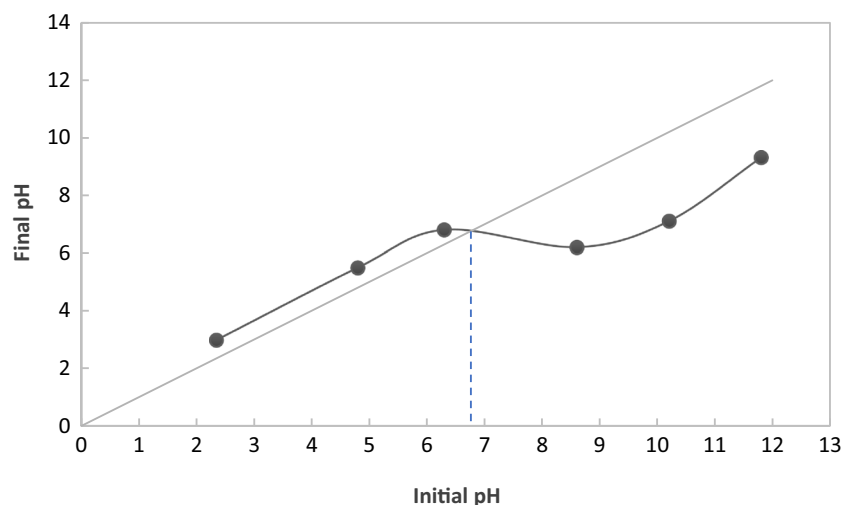
Table 3 Central composite design matrix for BR2 and MV removal

	No.	X_1 Initial dye concentration	X_2 pH	X_3 Temperature	X_4 Time	Y (BR2) adsorption percentage	Y (MV) adsorption percentage
Factorial points	1	−	−	−	−	56.88	63.91
	2	+	−	−	−	48.04	49.18
	3	−	+	−	−	91.36	93.26
	4	+	+	−	−	84.14	83.56
	5	−	−	+	−	58.45	62.53
	6	+	−	+	−	50.84	48.52
	7	−	+	+	−	93.38	95.32
	8	+	+	+	−	85.00	85.80
	9	−	−	−	+	57.78	64.61
	10	+	−	−	+	50.40	49.98
	11	−	+	−	+	93.51	94.21
	12	+	+	−	+	86.52	82.08
	13	−	−	+	+	60.17	64.61
	14	+	−	+	+	51.14	49.38
	15	−	+	+	+	94.36	96.13
	16	+	+	+	+	86.00	84.74
Axial points	17	− 2	0	0	0	80.74	84.00
	18	+ 2	0	0	0	64.00	59.00
	19	0	− 2	0	0	20.00	18.00
	20	0	+ 2	0	0	75.00	72.21
	21	0	0	− 2	0	77.79	83.00
	22	0	0	+ 2	0	77.59	82.55
	23	0	0	0	− 2	83.67	89.99
	24	0	0	0	+ 2	89.86	92.00
Central points	25	0	0	0	0	85.1	92.94
	26	0	0	0	0	86.31	93.69
	27	0	0	0	0	87.67	90.09
	28	0	0	0	0	89.80	95.20
	29	0	0	0	0	83.40	93.86
	30	0	0	0	0	84.29	92.86

Table 4 Estimated regression coefficient and corresponding t and p value for BR2 and MV

Factor	Parameter	BR2					MV				
		Regression coefficient	Effect	Standard error (SE)	t^a	ρ^b	Regression coefficient	Effect	Standard error (SE)	t^a	ρ^b
Model	a_0	86.09	86.09	1.12	76.34	0.00	93.10	93.10	0.81	114.93	0.00
X_1	a_1	−4.05	−8.10	1.12	−7.18	0.00	−6.34	−12.68	0.81	−15.65	0.00
X_1^2	a_{11}	−3.32	−6.64	1.05	−6.29	0.00	−5.32	−10.65	0.75	−14.06	0.00
X_2	a_2	16.27	32.54	1.12	28.85	0.00	15.41	30.83	0.81	38.05	0.00
X_2^2	a_{22}	−9.53	−19.07	1.05	−18.08	0.00	−11.92	−23.85	0.75	−31.47	0.00
X_3	a_3	0.42	0.85	1.12	0.76	0.64	0.18	0.37	0.81	0.46	0.65
X_3^2	a_{33}	−1.99	−3.98	1.05	−3.77	0.00	−2.50	−5.01	0.75	−6.62	0.00
X_4	a_4	1.00	2.01	1.12	1.78	0.39	0.35	0.70	0.81	0.87	0.39
X_4^2	a_{44}	0.27	0.55	1.05	0.52	0.24	−0.45	−0.90	0.75	−1.19	0.25
X_{12}	a_{12}	0.12	0.24	1.38	0.17	0.05	1.04	2.08	0.99	2.10	0.05
X_{13}	a_{13}	−0.18	−0.37	1.38	−0.27	0.81	0.11	0.23	0.99	0.23	0.82
X_{14}	a_{14}	0.02	0.04	1.38	0.03	0.44	−0.39	−0.78	0.99	−0.78	0.44
X_{23}	a_{23}	−0.27	−0.54	1.38	−0.39	0.14	0.77	1.54	0.99	1.55	0.14
X_{24}	a_{24}	0.08	0.15	1.38	0.11	0.45	−0.37	−0.75	0.99	−0.76	0.46
X_{34}	a_{34}	−0.23	−0.47	1.38	−0.34	0.91	0.05	0.11	0.99	0.11	0.91

[a] Value of the coefficient of regression for the error, measures it how big the effect is regarding the mistake standard or residue

[b] Probability of significance. If the level of confidence is 95% ρ value is 0.05 = 5% so that the result is significant

It was suggested from the statistical results (Table 4) that the initial dye concentration, the initial pH solution, and the temperature exhibited the most significant effects on the adsorption yield of BR2 and MV on raw date pits.

In order to evaluate the influence of the variable on the response, the magnitude and the sign of the regression coefficients were investigated. A synergistic effect can be highlighted by a positive sign while an antagonistic effect can be indicated by a negative sign.

A pareto chart diagram was used to investigate the standardized effects of the independent variables and their interactions on the dependent variable (Fig. 6). The standardized effects of factors on the response were evaluated by the length of each bar in the Pareto chart which is proportional to the importance of each corresponding factor (Solanki et al. 2007).

X_1, X_1^2, X_2, X_2^2, and X_3^2 are the significant terms which contributed the most in the prediction of BR2 and MV removal since the corresponding bars remained outside the reference line. An antagonistic effect of X_1, X_1^2, X_2^2, and X_3^2 model components on the BR2 and MV removal efficiency was highlighted from the corresponding negative coefficients. However, a synergistic effect of X_2 (pH) on the dyes removal efficiency was shown from its positive coefficients.

The removal of BR2 and MV was greater in basic pH range and decreased with acid pH. The low BR2 and MV adsorption at acid pH is due to the competition between excess H^+ ions and dye cations for the adsorption sites. In fact, BR2 and MV contains positive charge on the nitrogen atom which will strongly repels the positively charged adsorbent molecules at low pH since date pits are positively charged for pH < pH_{PZC} (6.8). At alkaline pH, the positively charged amine groups of date pits are diminished and the adsorption of BR2 and MV on date pits surface may be due to electrostatic attraction between the negatively charged surface of the adsorbent (COO^-, OH^-) and the cationic dyes which favors their adsorption.

The increase of the initial dye concentration leads to the reduction of the adsorption percentage. In fact, at high concentrations, the active sites of the adsorbent surface are occupied by dye molecules and the dyes removal from solution will be reduced. Moreover, the low adsorbent surface (S_{BET}) determined earlier can explain in part the saturation of adsorbent surface on high dye concentrations. On the other hand, the steric repulsion between dye molecules can slow down the adsorption process.

The significant quadratic coefficient of temperature contrary to his linear coefficient shows a non-linear variation of this factor. In fact, dye adsorption onto date pits increased up to about 94.36 and 96.13%, respectively, for BR2 and MV when the temperature was increased from 25 to 50 °C. Starting from this latter point until 62.5 °C, the increase is no longer as relevant. In fact, this result can be explained by the increase of the dye molecules mobility and the reduction of the retarding forces of dyes diffusion upon the increase of temperature. However, at the temperature of 62.5 °C, the attractive forces between dyes and adsorbent surface are weakened and a decrease of the dyes removal was highlighted.
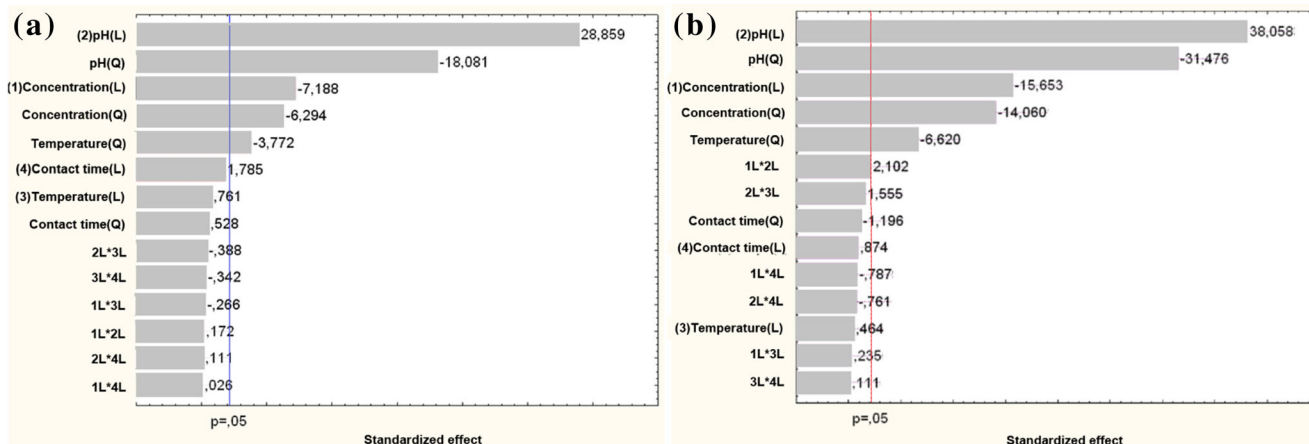
Fig. 6 Pareto chart showing the standardized effect of independent variables and their interaction on **a** BR2 and **b** MV removal efficiency

In the studied range, contact time (t) showed little effect with maximum removal efficiency obtained at $t = 150$ min. The rapid adsorption observed during the first 15 min is probably due to the abundant availability of the negatively charged surface (OH^-, COO^-) on the date pits surface, and with the gradual filling of these sites, the sorption becomes less efficient. This is the reason why an insignificant enhancement in BR2 adsorption is effected in 150 min (89.86 and 62%, respectively, for BR2 and MV) as compared to that in 30 min (83.67 and 89.99%, respectively, for BR2 and MV).

Determination of the regression model and statistical evaluation

A polynomial regression modeling was performed between the response variable, Y (adsorption percentage) and the coded values (X_1, X_2, X_3, X_4) corresponding to the four different process variables.

The fitted model equation for BR2 was given as below:

$$Y_{BR2} = 86.09 - 4.05X_1 - 3.32X_1^2 + 16.27X_2 - 9.53X_2^2$$

$$+ 0.42X_3 - 1.99X_3^2 + X_4 - 0.27X_4^2$$

$$+ 0.12X_{12} - 0.18X_{13} + 0.02X_{14} - 0.27X_{23}$$

$$+ 0.08X_{24} - 0.24X_{34} + 2.36 \quad (9)$$

The fitted model equation for MV was obtained as follows:

$$\text{For MV}: Y_{MV} = 93.10 - 6.34X_1 - 5.32X_1^2$$

$$+ 15.41X_2 - 11.92X_2^2$$

$$+ 0.18X_3 - 2.5X_3^2$$

$$+ 0.35X_4 - 0.45X_4^2 + 1.04X_{12}$$

$$+ 0.11X_{13} - 0.39X_{14}$$

$$+ 0.77X_{23} - 0.37X_{24} + 0.05X_{34}$$

$$+ 1.70 \quad (10)$$

The adequacy of the model was justified through analysis of variance (ANOVA) that tests the fitting of the second-order polynomial equation with the experimental data as given in Table 5. According to the Fisher's F-test, the large value of F indicates that most of the variation in the response can be explained by the regression model equation.

The calculated F value (F-ratio $_{R/r}$ equal to 398.98 and 109.1, respectively, for BR2 and MV) was found to be greater than the tabulated F ($F_{tab\ (0.05,\ 5,\ 24)} = 2.62$ for BR2 and $F_{tab\ (0.05,\ 14,\ 15)} = 2.46$ for MV) at the 5% level which indicate that the second-order polynomial model equations (Eqs. 8 and 9) were highly significant and adequate to represent the actual relationship between the response (percentage of adsorption) and the studied variables.

Moreover, ANOVA made the case that the model fits well the experimental data, since the calculated F-ratio $_{LOF/PE}$ are lower than the tabulated F value, respectively, for BR2 (F-ratio$_{LOF/PE} = 0.82$; $F_{0.05,19,5} = 4.60$) and MV (F-ratio$_{LOF/PE} = 3.48$; $F_{0.05,19,5} = 4.75$) at 95% of confidence.

The goodness of fit of the model was checked also by the analysis of residue which allows the determination of the coefficient (R^2).

Figure 7 reveals the distribution of the calculated values versus experimental values for the two responses corresponding to BR2 and MV adsorption. The points are almost randomly distributed about the line providing good agreements between experimental and calculated values using the quadratic model.

The value of determination coefficient (R^2) (0.988 and 0.994, respectively, for BR2 and MV) indicated that only 1.2% for BR2 and 0.5% for MV of the total variations do not stick with the regression model. Besides, a high significance of the model was highlighted by the high value of the adjusted coefficient R^2_a (0.976 and 0.989 for BR2 and MV, respectively).

Table 5 ANOVA for the fitted model

Source of variation	BR2					MV				
	SS	DF	MS	F-ratio	F-tab	SS	DF	MS	F-ratio	F-tab
R	9495.75	5	1899.15	398.98	2.62	11,731.85	14	837.99	109.10	2.46
r	114.47	24	4.76			115.21	15	7.68		
LOF	86.70	19	4.56	0.82	4.60	100.73	10	10.073	3.48	4.75
PE	27.76	5	5.52			14.48	5	2.89		
Total	9610.22	29				11,847.07	29			

R regression, *r* residual, *LOF* lack of fit, *PE* pure error, *SS* sum of square, *DF* degree of freedom, *MS* mean square

Optimization removal efficiency

A quadratic regression model was implemented so as to optimize the leading variables by maximizing the BR2 and MV removal by date pits. Considering the results of *p* values (Table 4) and the pareto chart (Fig. 6), the empirical regression models of BR2 and MV could be simplified as follows:

$$Y_{BR2} = 88.44 - 4.05X_1 - 3.32X_1^2$$
$$+ 16.27X_2 - 9.53X_2^2 - 1.99X_3^2 \quad (11)$$

$$Y_{MV} = 94.80 - 6.34X_1 - 5.32X_1^2$$
$$+ 15.41X_2 - 11.92X_2^2 - 2.50X_3^2 \quad (12)$$

Solving these two latter equations and plotting the response surface contour allowed us to get the optimum values of the major effect variables.

The optimal values of the test variables in coded units were calculated by an algorithm, and the natural values were then determined by replacing the respective coded values in Eq. (3). Coded and natural values of the significant variables influencing the BR2 and MV adsorption and their maximum removal percentage (*Y*) were summarized in Table 6.

Response surface contour plots were carried out also to determine the optimal conditions for a maximal BR2 and MV adsorption using STASTICA (Trial version 9.0, StatSoft Inc., USA) software package. The 3D response surface diagrams were presented for the most influencing variables (pH and concentration) (Fig. 8).

The stationary point also called central point corresponds to the point where the slope of the contour is nil in all directions. Its coordinates within the highest contour levels allows to get the optimum values of the respective constituents (Ravikumar et al. 2005) (Fig. 8).

The maximum predicted yield is indicated by the surface confined in the smallest curve of the contour diagram (Gopal et al. 2002).

Kinetic adsorption of BR2 and MV on date pits under optimum conditions

Adsorption kinetics are performed and the results are presented in Fig. 9, where the dye concentration on adsorbent (q_t) was plotted against time.

It is clear from experimental kinetic results that the sorption capacity increases with an increase in contact time and reaches a plateau almost at 60 and 30 min for BR2 and MV, respectively. Additionally, the high sorption rate on the first stage of dyes uptake especially for MV can be explained by the high availability of the free functional groups on adsorbent surface which decline with time. Similar trends have been reported by Aljeboree et al. (2017) who studied the adsorption of maxilon blue and direct yellow by activated carbon derived from coconut shell. Moreover, Mohanty et al. (2006) studied the effect of contact time on MV uptake by activated carbon prepared from rice husk and it was noticed that the sorption rate was rapid on the first stage and became constant after a period of 120 min for the different studied concentrations (50, 150, and 250 mg L^{-1}). Similarly, it was highlighted by Miyah et al. (2017) that 80% of MV was adsorbed by clay after a contact time of 10 min and the overall reaction time was fixed to 120 min.

Similar contact times (2 h) were used Mohanty et al. (2006), who studied MV adsorption onto activated carbon prepared from Rice husk, as the sorption remained constant after a period of 120 min for concentrations ranging between 50 and 250 mg/L. A contact time of 1 h was applied by Mahmoudi et al. (2015) who studied the uptake of methylene blue and methyl orange by raw Tunisian date pits. The authors demonstrated that the contact time necessary to reach equilibrium on the removal of both dyes with initial concentrations of 500 mg/L was 1 h for raw date pits contrarily to activated carbon which needs longer equilibrium time of 10 h.

In order to estimate the sorption rate of BR2 and MV uptake onto date pits, pseudo-first- and pseudo-second-order models were applied as these are the most used models to fit kinetic data. Pseudo-first- (Lagergren 1898) and pseudo-second-order (Ho and McKay 1999) models were represented by Eqs. (13) and (14), respectively.
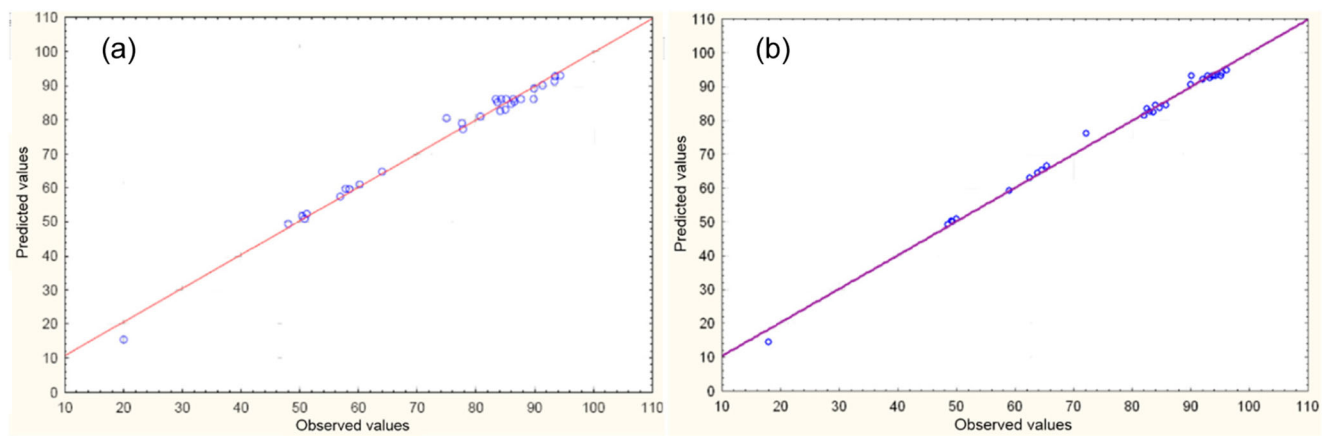
Fig. 7 Calculated versus experimental values plot for **a** BR2 and **b** MV removal

$$q_t = q_e[\text{Exp}(\ln q_e - k_1 t)] \qquad (13)$$

$$q_t = \frac{q_e^2 k_2 t}{q_e k_2 t + 1} \qquad (14)$$

where q_t is the amount of dye adsorbed (mg/g) at time t (min), q_e is the amount of dye adsorbed at equilibrium (mg/g), k_1 (min^{-1}) is the pseudo-first-order rate constant and k_2 (mg g^{-1} min^{-1}) is the pseudo-second-order rate constant.

The pseudo-first-order and the pseudo-second-order models were are displayed in Fig. 9.

The linear form of pseudo-first- and pseudo-second-order models were used to determine the kinetic constants.

Rate constants (k_1 and k_2), predicted equilibrium uptakes, and correlation coefficients R^2 were summarized in Table 7.

According to Table 7, the low values of R^2 (0.298 and 0.285 for BR2 and MV, respectively) for pseudo-first-order model indicated that this model failed to describe the kinetic uptake of BR2 and MV onto date pits. However, pseudo-second-order model was found to be able to predict experimental data since R^2 values were close to unity for both dyes (0.999 and 1 for BR2 and MV, respectively). This finding was further confirmed by the predicted equilibrium sorption capacities $q_{e,2}$ (57.14 and 59.52 mg g^{-1}, respectively, for BR2 an MV) which were found similar to experimental values $q_{e,exp}$ (56 and 59.35 mg g^{-1} for BR2 and MV, respectively).

Similar results were reported in the works of Chandane and Sing (2014) and Miyah et al. (2017) who studied the uptake of BR2 and MV onto soybean hull and clay, respectively. They showed that pseudo-second-order model was the best fitted model compared to the pseudo-first-order model.

Since the pseudo-first- and the pseudo-second-order models do not allow to understand the adsorption mechanism, intraparticle diffusion model, known as Weber and Morris model, was investigated to determine the controlling step in adsorption process. Intraparticle diffusion model is expressed as follows (Weber and Morris 1963):

$$q_t = k_{in} t^{1/2} + C \qquad (15)$$

where q_t (mg g^{-1}) is the amount adsorbed at time t, k_{in} is the intraparticle rate constant (mg min$^{0.5}$ g^{-1}), and C is the intercept (mg g^{-1}).

The kinetic parameters of the intraparticle diffusion model were generally determined by plotting (q_t) vs. time (min$^{0.5}$). The intraparticle rate constant (K_{in}) as well as the intercept C were determined respectively from the slope and the intercept of the curve according to Weber and Morris equation (Eq. 15).

As shown in Table 7, C values were not equal to zero, suggesting that intraparticle diffusion of BR2 and MV was not the sole rate controlling step and it can be associated with other transfer resistance.

The comparison of intercept values corresponding to BR2 (37.36 mg/g) and MV (53.75) showed that the latter dye

Table 6 Optimum coded and uncoded values of significant variables for BR2 and MV

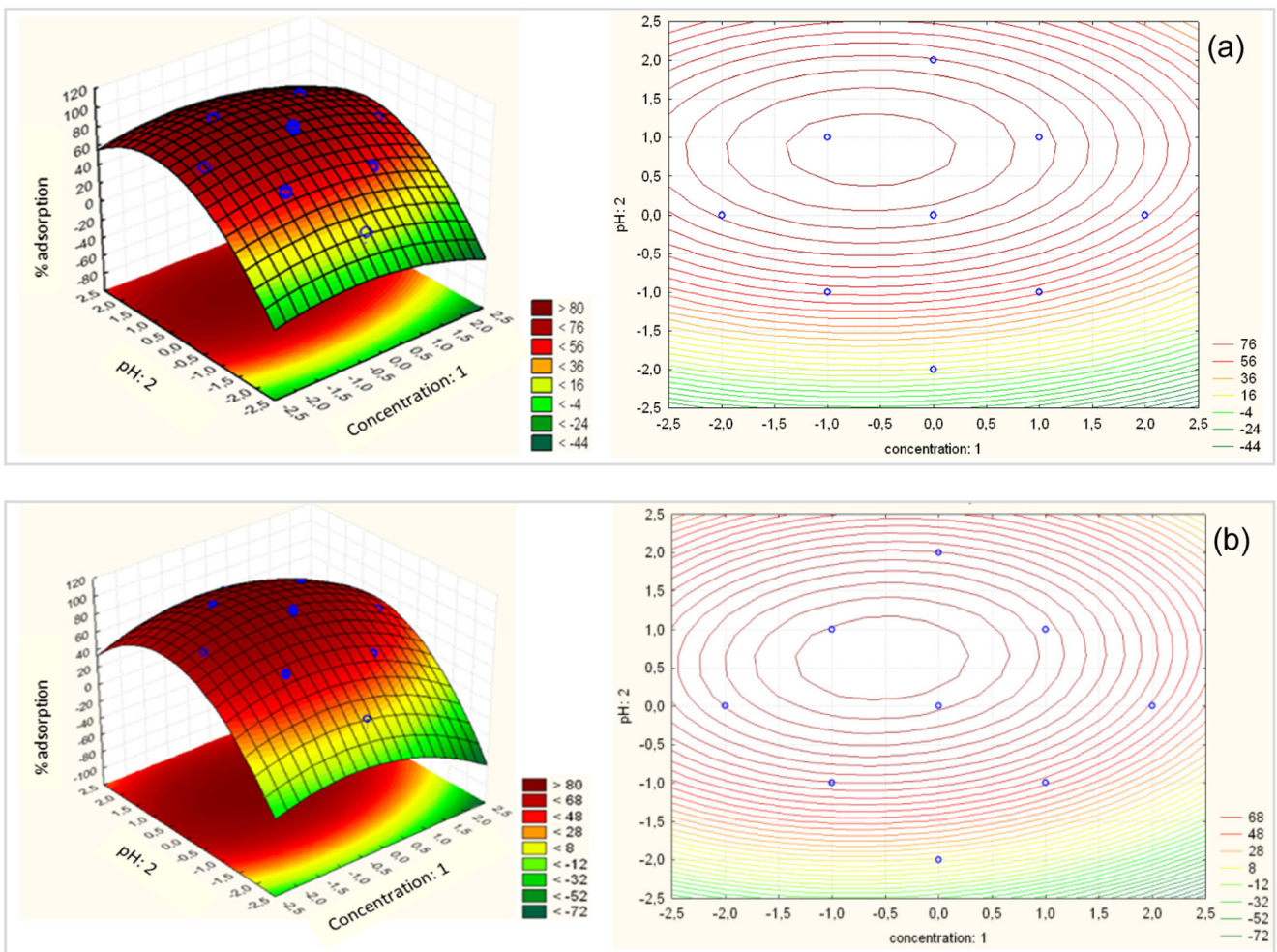|	BR2		MV	
	Coded values (x)	Natural values (X)	Coded values (x)	Natural values (X)
Initial concentration (mg L^{-1})	− 0.60	59.77	− 0.59	60.25
PH	0.85	7. 70	0.64	7.28
Temperature (°C)	0.10	38.75	0.038	37.96
Maximum removal percentage Y (%)	96.66		100	

Fig. 8 3D response surface diagrams showing the effects of the mutual interactions between two independent variables on **a** BR2 and **b** MV adsorption

Fig. 9 Experimental and theoretical kinetic data of BR2 and MV adsorption on date pits
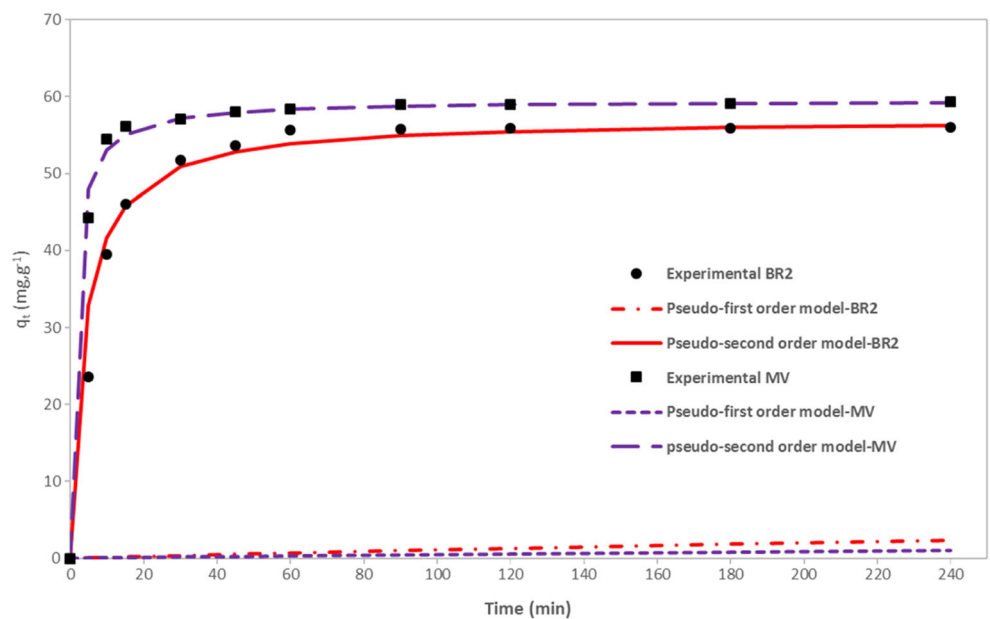
Table 7 Rate parameters of pseudo-first-order, pseudo-second-order, and intraparticle diffusion models for BR2 and MV uptake on date pits

	Experimental	Pseudo-first-order model			Pseudo-second-order model			Intraparticle diffusion model		
	$q_{e,exp}$ (mg g^{-1})	$q_{e,1}$ (mg g^{-1})	k_1 (min^{-1})	R^2	$q_{e,2}$ (mg g^{-1})	k_2 (mg g^{-1} min^{-1})	R^2	k_{in}	C (mg g^{-1})	R^2
BR2	56	6.43	0.0019	0.298	57.14	0.005	0.999	2.42	37.36	0.964
MV	59.35	7.33	0.0006	0.285	59.52	0.014	1	0.61	53.75	0.987

exhibited higher resistance to transfer in the film surrounding particles.

On the other hand, as seen in Table 7, the intraparticle rate constant was higher for BR2 (2.42 mg min$^{0.5}$ g^{-1}) than for MV (0.61 mg min$^{0.5}$ g^{-1}) indicating that MV was more hindered to diffuse inside particles compared to BR2.

Thus, it can be concluded from kinetic results that pseudo-second order was able to describe successfully the kinetic data of BR2 and MV. Moreover, it was suggested from Weber and Morris model that intraparticle diffusion mechanism is not the sole limiting mechanism and it was associated with other controlling step such as film diffusion. Additionally, the transfer resistance onto date pits adsorbent was higher for MV compared to BR2.

Adsorption isotherm of BR2 and MV on date pits under optimum conditions

Experimental results

Equilibrium isotherm is a plot of the quantity of the sorbate removed per unit sorbent (q_e) versus the concentration of the sorbate in the liquid phase (C_e) (Fig. 10).

The amount of dye adsorbed per unit mass of the pits goes up with the dye initial concentration to reach the plateau values indicating thus a saturation of the active sites. For both dyes, experimental isotherms showed an L-shape adsorption according to the classification of Giles et al. (1974). This
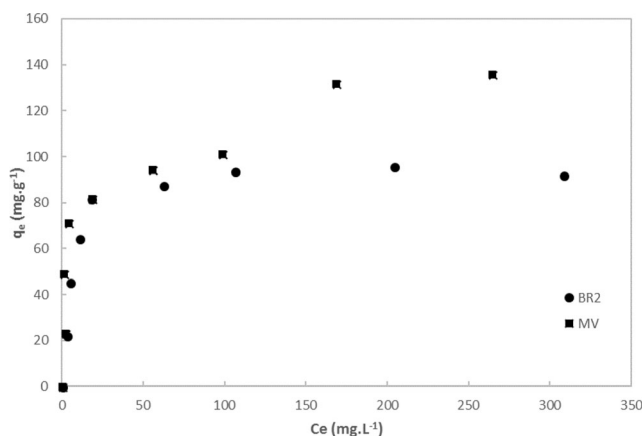
Fig. 10 Experimental adsorption isotherm of BR2 and MV by date pits ($C_0 = 25$–400 mg L^{-1}, contact time = 2 h, temperature = 35 °C, pH$_{BR2}$ = 7.7; pH$_{MV}$ = 7.28)

means that there is no strong competition between the solvent and dyes for date pits surface sites (Muruganaadham and Swaminathan 2004; Bouberka et al. 2009).

Moreover, one can see that adsorption rate was higher for MV (136 mg g^{-1}) than for BR2 (92 mg g^{-1}).

The difference in maximum adsorption capacity between the studied dyes can be explained by the higher affinity of MV for date pits particles. In fact, this affinity can be attributed to the low solubility of MV (16 g L^{-1}) in comparison to BR2 (50 g L^{-1}).

On the other hand, adsorption capacities of BR2 and MV on date pits were compared to other low-cost adsorbents (Table 8).

It can be clearly seen that adsorption capacities of MV and BR2 on date pits were superior to most natural adsorbents recently tested in the literature (skin almond waste, maize silk,..). This can be attributed to its physicochemical properties (functional groups..).

Adsorption isotherm models and error analysis

Modeling isotherms is important to predict and compare adsorption performance. Five two-parameter isotherm models are used to fit the experimental results of BR2 and MV adsorption on date pits (Langmuir, Freundlich, Temkin, Dubinin–Radushkevich, and Halsay models). The main purpose of this section is to recommend the best descriptive isotherm equation by error analysis.

- *Langmuir model*

The main assumptions in Langmuir sorption model are (a) maximum adsorption capacity consists of a monolayer adsorption, (b) there are no interactions between adsorbed molecules, and (c) the adsorption energy is equally distributed over the entire coverage surface (Santhi et al. 2010; Subramani and Thinakaran 2017; Madrakian et al. 2015). The Langmuir isotherm is expressed as follows (Langmuir 1918):

$$q_e = \frac{q_{max} \cdot K_L \cdot C_e}{1 + K_L \cdot C_e} \quad (16)$$

where q_e (mg g^{-1}) and q_{max} (mg g^{-1}) are respectively the amount and the maximum amount of dye adsorbed per unit

Table 8 Adsorption capacities of different adsorption systems

Adsorbents	Dyes	Adsorption capacities (mg g^{-1})	References
Raw date pits	Methyl violet	136.00	This work
Raw date pits	Basic red 2	92.00	This work
Natural porcellanite	Basic red 2	66.22	(Samaka 2014)
Skin almond waste	Méthyl violet	85.47	(Atmani et al. 2009)
Maize silk	Methylene blue	65.00	(Miraboutalebi et al. 2017)

mass of adsorbent, C_e (mg L^{-1}) is the concentration of the adsorbate at equilibrium, and K_L (L mg^{-1}) is Langmuir constant related to the affinity of the binding sites (Ahmad et al. 2009).

The linear form of Langmuir isotherm equation allows to get q_{max} and K_L.

Webi and Chakravort (1974) expressed the Langmuir isotherm in term of dimensionless constant separation factor or equilibrium parameter (R_L) defined by:

$$R_L = \frac{1}{1 + K_L \cdot C_0} \tag{17}$$

where C_0 is still the initial dye concentration (mg L^{-1}).

R_L coefficient assumes the nature and the feasibility of adsorption process and indicates the type of isotherm to be irreversible ($R_L = 0$), favorable ($0 < R_L < 1$), linear ($R_L = 1$), or unfavorable ($R_L > 1$).

• *Freundlich model*

The Freundlich isotherm model is an empirical expression which describes the non-ideal and reversible adsorption (Freundlich 1906) and that can be applied to multilayer adsorption, with non-uniform distribution of adsorption heat and affinities over the heterogeneous surface (Foo and Hameed 2012). The Freundlich equation is given by the following:

$$q_e = K_F \cdot C_e^{1/n} \tag{18}$$

where K_F (L g^{-1}) and n are the Freundlich constants, indicating respectively the adsorption capacity and the adsorption intensity.

The plot of log q_e versus log C_e helps getting the intercept K_F and the slope $1/n$.

• *Temkin model*

Temkin isotherm considers that the heat of adsorption is reduced linearly with the coverage due to adsorbate-adsorbent interactions (Vijayaraghavan et al. 2006; Wang 2013). The corresponding equation is given below (Tempkin and Pyzhev 1940):

$$q_e = \frac{RT}{b_T} \ln (K_T \cdot C_e) \tag{19}$$

where K_T (L mg^{-1}) is the Temkin isotherm constant, b_T (J mol^{-1}) is a constant related to heat of sorption, R is the ideal gas constant (8.314 J/mol K), and T is absolute temperature (308.15 K).

A plot of q_e against ln C_e enables having b_T and K_T.

• *Dubinin–Radushkevich model*

Dubinin–Radushkevich isotherm assumes that the sorption curves are related to the adsorbent porous structure and its equation is given by (Dubinin 1960; Abdelwahab 2007; Mohamed and Ouki 2011):

$$q_e = q_m \, Exp \left(-\beta \varepsilon^2\right) \tag{20}$$

where q_m is the maximum sorption capacity (mg g^{-1}), and β is the Dubinin–Radushkevich constant (mol^2 KJ^{-2}).

$$\varepsilon = RT \ln \left(1 + \frac{1}{C_e}\right) \tag{21}$$

β is related to the mean free energy of sorption per mole E of adsorbate during its transfer and can be determined by the above equation (Hasany and Chaudhary 1996; Samarghandi et al. 2009):

$$E = \frac{1}{\sqrt{2\beta}} \tag{22}$$

The magnitude of mean free energy of adsorption give an information about whether the adsorption mechanism is physical or chemical (Erdem et al. 2004). In fact, if the mean free energy is more than 8 KJ mol^{-1}, the adsorption process is governed by chemisorption, whereas if it is lower, physical phenomena occur (Lodeiro et al. 2006; Kilislioglu and Bilgin 2003).

• *Halsay model*

As Halsay isotherm reveals the heterosporous nature of the adsorbent, it is more suitable for multilayer adsorption (Halsey

Table 9 Names and equations of the applied error functions

Error function	Equation	Equation no.
Residual root mean square error (RMSE)	$$\sqrt{\frac{1}{N-2}\sum_{i=1}^{N}\left(q_{e,exp}-q_{e,isotherm}\right)^2}$$	(24)
Chi-square statistic (χ^2)	$$\sum_{1}^{N}\frac{\left(q_{e,exp}-q_{e,isotherm}\right)^2}{q_{e,isotherm}}$$	(25)
Average relative error (ARE)	$$\sum_{i=1}^{N}\left|\frac{q_{e,exp}-q_{e,isotherm}}{q_{e,exp}}\right|$$	(26)

$q_{e,exp}$ and $q_{e,isotherm}$ are respectively the experimental and the calculated values of q_e; N is the number of experiments

1952; Sampranpiboon et al. 2014). The relevant equation is (Halsey 1952):

$$q_e = \mathrm{Exp}\left(\frac{\ln K_{Ha}-\ln C_e}{n_{Ha}}\right) \tag{23}$$

where K_{Ha} (mg L^{-1}) and n_{Ha} are the Halsay isotherm constant and exponent, respectively.

For the five isotherms defined in this section, model parameters were determined (Table 9) and q_e values were calculated and plotted against C_e.

Fig. 11 Experimental data and predicted isotherms of BR2 (**a**) and MV (**b**) adsorption on date pits according to Langmuir, Freundlich, Temkin, Dubinin–Radushkevich, and Halsay models
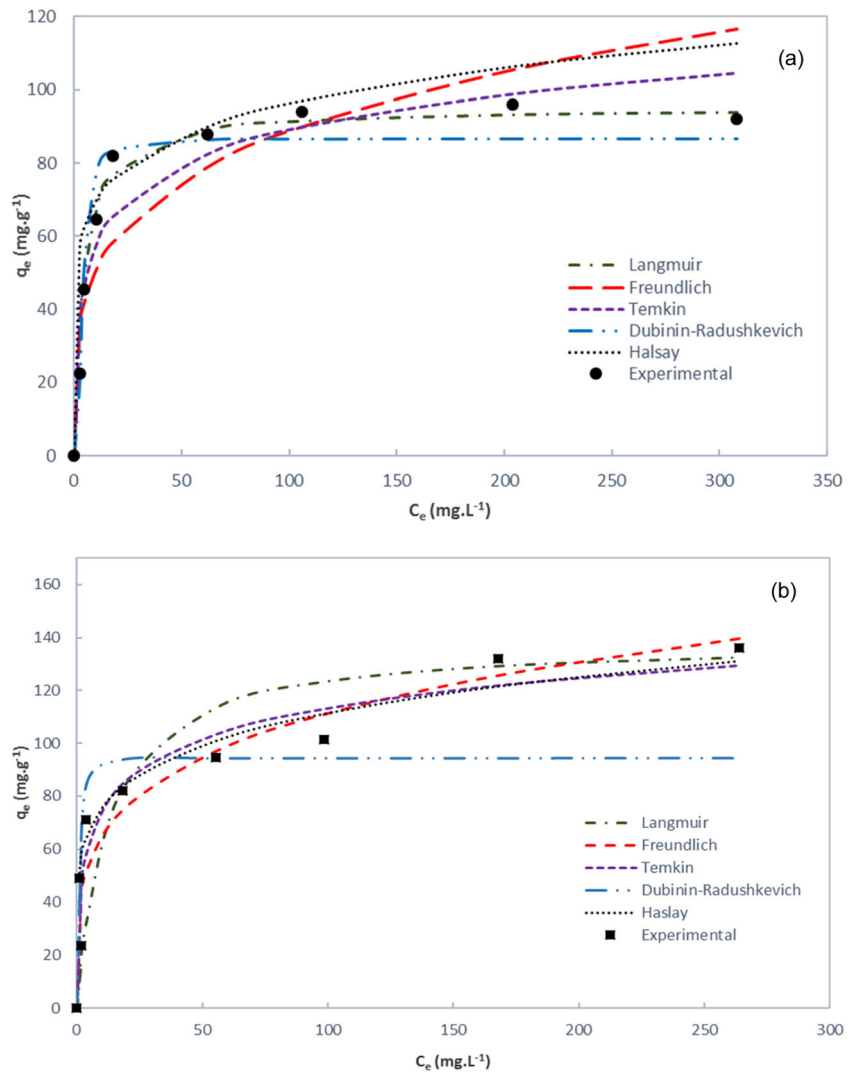
Table 10 BR2 and MV adsorption onto date pits at equilibrium and their fitting by Langmuir, Freundlich, Temkin, Dubinin–Radushkevich, and Halsay isotherm models

Isotherm model	Parameters	Basic red 2	Methyl violet
Langmuir	Q_{max} (mg g^{-1})	95.24	138.89
	K_L (L mg^{-1})	0.23	0.08
	R^2	0.97	0.84
	RMSE	6.31	25.7
	χ^2	5.79	211.82
	ARE	0.86	2.13
Freundlich	n	4.11	4.28
	K_F (L g^{-1})	28.91	37.91
	R^2	0.842	0.94
	RMSE	17.02	13.43
	χ^2	26.07	21.59
	ARE	1.71	1.61
Temkin	b_T (J mol^{-1})	186.08	153.07
	K_T (L mg^{-1})	6.46	8.64
	R^2	0.91	0.93
	RMSE	11.52	13.87
	χ^2	13.96	21.30
	ARE	1.32	1.72
Halsay	n_{Ha}	−7.12	−5,96
	K_{Ha} (mg L^{-1})	$7.45 \ 10^{-13}$	$6.395 \ 10^{-11}$
	R^2	0.82	0.9
	RMSE	18.84	15.13
	χ^2	31.81	22.04
	ARE	2.48	1.83
Dubinin–Radushkevich	q_m (mol g^{-1})	86.71	94.23
	β (mol^2 KJ^{-2})	2	0.3
	E (KJ mol^{-1})	0.5	1.29
	R^2	0.96	0.59
	RMSE	7.91	29.12
	χ^2	4.86	66.56
	ARE	0.65	2.86

Figure 11a, b compare the theoretical isotherm curves of Langmuir, Freundlich, Temkin, Dubinin–Radushkevich, and Halsay models with the experimental data of BR2 and MV adsorption onto date pits.

Figure 11a shows an excellent fit of Langmuir model with experimental data for the removal of BR2 for all the range of studied concentrations. It should be mentioned that Dubinin–Radushkevich model describes well experimental results namely on the low concentrations. Temkin, Freundlich, and Halsey models did not match experimental data as far as BR2 removal is concerned.

As seen in Fig. 11b, Temkin, Freundlich, and Halsey models predict better MV adsorption when compared to Langmuir and Dubinin–Radushkevich models. In fact, this latter model underestimates the adsorption capacity (q_e) in

the range of high concentrations contrarily to Langmuir model which overestimates q_e on the range of lower concentrations.

To check the consistency of the adsorption isotherm models, an error analysis study should be conducted.

- *Error analysis*

In order to determine the most accurate isotherm constant parameters and to identify the model with the best fit, residual root mean square error (RMSE), chi-square statistic (χ^2), and average relative error (ARE) values were calculated using Eqs. (24), (25), and (26), respectively (Ip et al. 2009; Miraboutalebi et al. 2017; Ramteke and Gogate 2016) (Table 9).

The smaller are the RMSE, χ^2, and ARE values, the better is the curve fitting. Whereas, the closer correlation coefficient (R^2) values to unity, the better is the fitting.

For each studied model and for each dye, the values of isotherm parameters RMSE, χ^2, and ARE as well as the (R^2) are presented in Table 10.

According to the error results of BR2, the Langmuir and Dubinin–Radushkevich models are the most appropriate to describe the adsorption process of BR2, where R^2 (0.97 and 0.96) are the highest and RMSE (6.31 and 7.91), chi-square statistic (5.79 and 4.86), and ARE (0.86 and 0.65) are the lowest, respectively. However, Freundlich, Temkin, and Halsay models were ranked the worst isotherms for fitting the adsorption of BR2 on date pits.

Similar findings were reported by Samarghandi et al. (2009) when they studied the removal of methyl orange by pinecone-derived activated carbon. It was shown that Dubinin–Radushkevich and Langmuir models reveal a better agreement with experimental data.

One can also see that RMSE (18.84), χ^2 (31.81), and ARE (2.48) in Halsay model are quite high when compared to other models. One can conclude that not only Halsay model is not appropriate to describe BR2 sorption by date pits but also and mainly that the hypothesis of multilayer adsorption cannot be assumed.

For BR2, as Langmuir isotherm fits experimental data, one can affirm that once a dye occupies a site, no further adsorption can take place at that site and that the adsorbent surface is energetically homogeneous.

The values of dimensionless Langmuir separation factor (R_L) for BR2 removal were calculated (Eq. 17) for the range of the studied initial concentrations (25–400 mg L^{-1}). The values of R_L for BR2 adsorption on the date pits were greater than zero and less than 1, indicating favorable adsorption ($0.01 < R_L < 0.15$). The maximum adsorption capacity determined by Langmuir model (92 mg g^{-1}) was almost close to the experimental adsorption capacity of BR2 onto date pits (95.24 mg g^{-1}) (Table 10).

The Dubinin–Radushkevich model gives an idea about the nature of sorption by calculating the mean free energy (Eq. 22). This latter (0.5 KJ mol^{-1}) was found to be lower than 8 KJ mol^{-1}, making us think BR2 removal as a physisorption mechanism.

Analogous results were reported in the work of Ibrahim and Sani (2014) who investigated Congo red removal by watermelon rinds and neem tree leaves. Dubinin–Radushkevich model reveals a good fit to experimentation and it confirmed a physical adsorption process.

Contrarily to the BR2 fitting results and according to error analysis funding, MV adsorption data fitting shows that Freundlich, Temkin, and Halsey models provide better concordance in comparison with Dubinin–Radushkevich and Langmuir. These latter models exhibited respectively the lower correlation coefficients R^2 (0.84 and 0.59) and the higher values of RMSE (25.7 and 29.12), chi-square statistic (211.82 and 66.56), and ARE (2.13 and 2.86) (Table 10).

The values of R^2 (0.94 and 0.93), RMSE (13.43 and 13.87), χ^2 (21.59 and 21.30), and ARE (1.61 and 1.72) seen in Table 9 for Freundlich and Temkin models are close and all of them are better than those of Halsay.

The poor fitting of Langmuir and Dubinin–Radushkevich models to experimental data could explain that the monolayer adsorption of MV does not occur and probably a multilayer behavior for the sorption of a MV onto adsorbent could be highlighted as in the assumption of Halsay model.

The magnitude of Freundlich constant K_F (37.91) showed a high MV adsorptive capacity from aqueous solution. Furthermore, from Table 9, Freundlich constant, n is equal to 4.28, indicating favorable adsorption of MV by date pits, as it is ranged between 1 and 10 (Freundlich 1906). It was reported in earlier studies that a $(1/n)$ value below 1 implies chemisorption process; otherwise, it is rather a cooperative mechanism (Brasquet et al. 1997; Shahbeig et al. 2013). Keeping this in mind, MV sorption is again thought to be chemical, with the establishment of strong bonding between dye molecules and the functional sites of the heterogeneous surface.

Conclusions

A thorough examination of literature revealed that date stones were never used as adsorbent of BR2 and MV, and the present study aimed then to optimize process variables in order to maximize the removal of these cationic dyes from aqueous phase and to measure the adsorption capacity of the date pits in optimum conditions. The RSM-CCD was applied to determine the effect and the interaction between four different operating parameters (temperature, pH, initial dye concentration, and contact time). A second-order quadratic model used in response surface analysis brought that pH and initial dye concentration are the most influent variables. The R^2 values of the response parameters showed a good fit of the model with experimental data. The optimum process conditions were determined by solving the quadratic models.

Kinetic results suggested that BR2 and MV adsorption processes obeyed to pseudo-second-order kinetic model and intraparticle diffusion model played significant role on sorption mechanism but was not the sole controlling step.

Equilibrium isotherms were determined in optimum conditions and experimental adsorption capacities were 92 and 136 mg g^{-1} for BR2 and MV, respectively.

Error analysis did uphold that Langmuir and Dubinin–Radushkevich models offer high accuracy for predicting the adsorption behavior of BR2 adsorption contrarily to Freundlich, Temkin, and Halsay models. However, the equilibrium fitting results of MV suggested Freundlich, Temkin, and Halsay models match.

According to these findings, it appears that MV and BR2 are well removed from water by date pits but with different mechanisms. In fact, it is a monolayer adsorption process controlled by physisorption for BR2, whereas it is rather multilayer-chemisorption for MV.

References

Abdelwahab O (2007) Kinetic and isotherm studies of copper (II) removal from wastewater using various adsorbents. Egypt J Aquat Res 33: 125–143

Adegoke KA, Bello OS (2015) Dye sequestration using agricultural wastes as adsorbents. Water Res Ind 12:8–24

Adinarayana K, Ellaiah P (2002) Response surface optimization of the critical medium components for the production of alkaline protease by a newly isolated Bacillus sp. J Pharm Pharm Sci 5:272–278

Ahmad AA, Hameed BH, Ahmad AL (2009) Removal of disperse dye from aqueous solution using waste-derived activated carbon: optimization study. J Hazard Mater 170:612–619

Ahmed MJ, Theydan SK (2014) Adsorptive removal of p-nitrophenol on microporous activated carbon by FeCl3 activation: equilibrium and kinetics studies. Desalin Water Treat 670:1–10

Alam Z, Muyibi SA, Toramae J (2007) Statistical optimization of adsorption processes for removal of 2,4-dichlorophenol by activated carbon derived from oil palm empty fruit bunches. J Environ Sci 19: 674–677

Al-Ghouti MA, Hawari A, Khraisheh M (2013) A solid-phase extractant based on microemulsion modified date pits for toxic pollutants. J Environ Manag 130:80–89

Al-Ghouti MA, Al Disi ZA, Al-Kaabi N, Khraisheh M (2017) Mechanistic insights into the remediation of bromide ions from desalinated water using roasted date pits. Chem Eng J 308:463–475

Aljeboree AM, Alshirifi AN, Alkaim AF (2017) Kinetics and equilibrium study for the adsorption of textile dyes on coconut shell activated carbon. Arab J Chem 10:3381–3393

Amor HB, Ismail M (2015) Adsorption of chromium (VI) on activated carbon prepared by acid activation of date stones. Int J Sci Res 4:309–314

Arami M, Limaee NY, Mahmoodi NM, Tabrizi NS (2006) Equilibrium and kinetics studies for the adsorption of direct and acid dyes from aqueous solution by soy meal hull. J Hazard Mater 135:171–179

Ardejani K, Doulati N, Badii NM, Yousefi Limaee M, Mahmoodi SZ, Arami AR, Mirhabibi S (2007) Numerical modelling and laboratory studies on the removal adsorption technique for the removal of organic pollutants from water and wastewater of direct red 23 and direct red 80 dyes from textile effluents using orange peel, a low-cost adsorbent. Dyes Pig 73:178–185

Ashour SS (2010) Kinetic and equilibrium adsorption of methylene blue and remazol dyes onto steam-activated carbons developed from date pits. J Saudi Chem Soc 14:47–53

Atmani F, Bensmaili A, Mezenner NY (2009) Synthetic textile effluent removal by skin almond waste. J Environ Sci Technol 2:153–169

Ayhan D (2009) Agricultural based activated carbons for the removal of dyes from aqueous solutions: a review. J Hazard Mater 167:1–9

Banat F, Al-Asheh S, Al-Ahmad R, Bni-Khalid F (2007) Bench-scale and packed bed sorption of methylene blue using treated olive pomace and charcoal. Bioresour Technol 98(16):3017–3025

Benaissa H (2010) Influence of ionic strength on methylene blue removal by sorption from synthetic aqueous solution using almond peel as a sorbent material: experimental and modelling studies. J Taibah Univ Sci 4:31–38

Bhaumik R, Mondal NK (2016) Optimizing adsorption of fluoride from water by modified banana peel dust using response surface modelling approach. Appl Water Sci 6:115–135

Bohli T, Ouederni A, Fiol N, Villaescusa I (2015) Evaluation of an activated carbon from olive stones used as an adsorbent for heavy metal removal from aqueous phases. C R Chim 18:88–99

Bouberka Z, Khenifi A, Ait Mahamed H, Haddou B, Belkaid N, Bettahar N, Derriche Z (2009) Adsorption of Supranol Yellow 4 GL from aqueous solution by surfactant-treated aluminum/chromium-intercalated bentonite. J Hazard Mater 162:378–385

Brasquet C, Subrenat E, Cloirec P (1997) Selective adsorption on fibrous activated carbon of organics from aqueous solution: correlation between adsorption and molecular structure. Water Sci Technol 35(7):251–259

Briones R, Serrano L, Younes RB, Mondragon I, Labidi J (2011) Polyol production by chemical modification of date seeds. Ind Crop Prod 34:1035–1040

Chandane V, Sing VK (2014) Adsorption of safranin dye from aqueous solutions using a low-cost agro-waste material soybean hull. Desalin Water Treat 57(9):4122–4134

Das P, Banerjee P, Mondal S (2015) Mathematical modelling and optimization of synthetic textile dye removal using soil composites as highly competent liner material. Environ Sci Pollut Res 22:1318–1328

Dubinin MM (1960) The potential theory of adsorption of gases and vapors for adsorbents with energetically non-uniform surface. Chem Rev 60:235–266

El-Naas MH, Al-Zuhair S, Alhaija MA (2010) Removal of phenol from petroleum refinery wastewater through adsorption on date-pit activated carbon. Chem Eng J 162:997–1005

Emanuele Lessa F, Gularte MS, Garcia ES, Fajardo AR (2017) Orange waste: a valuable carbohydrate source for the development of beads with enhanced adsorption properties for cationic dyes. Carbohydr Polym 157:660–668

Erdem E, Karapinar N, Donat R (2004) The removal of heavy metal cations by natural zeolites. J Colloid Interface Sci 280:309–314

Farinella NV, Matos GD, Arruda MAZ (2007) Grape bagasse as a potential biosorbent of metals in effluent treatment. Bioresour Technol 98:1940–1946

Ferrero F (2007) Dye removal by lowcost adsorbents: hazelnut shells in comparison with wood sawdust. J Colloid Interface Sci 142:144–152

Foo KY, Hameed B (2012) Preparation, characterization and evaluation of adsorptive properties of orange peel based activated carbon via microwave induced K2CO3 activation. Bioresour Technol 104:679–686

Freundlich H (1906) Over the adsorption in solution. J Phys Chem 57:385–471

Garbaa ZN, Rahima AA, Belloc BZ (2015) Optimization of preparation conditions for activated carbon from Brachystegia eurycoma seed hulls: a new precursor using central composite design. J Environ Chem Eng 3:2892–2899

Giles CH, Silva APD, Easton IA (1974) General treatment and classification of the solute adsorption isotherm. Colloid Interface Sci 47:766–778

Gnanasambandam R, Protor A (2000) Determination of pectin degree of esterification by diffuse reflectance Fourier transform infrared spectroscopy. Food Chem 68:327–332

Gopal M, Pakshirajan K, Swaminathan T (2002) Heavy metal removal by biosorption using Phanerochaete chrysosporium. Appl Biochem Biotechnol 102:227–237

Guibaud G, Tixier N, Bouju A, Baudu M (2003) Relationship between extracellular polymer's composition and its ability to complex Cd, Cu and Ni. Chemosphere 52:1701–1710

Halsey GD (1952) The role of surface heterogeneity. Adv Catal 4:259–269

Hasany SM, Chaudhary MH (1996) Sorption potential of hare rivers and for the removal of antimony from acidic aqueous solution. Appl Rad Isot 47:467–471

Hashem A, Akasha RA, Ghith A, Hussein DA (2007) Adsorbent based on agricultural wastes for heavy metal and dye removal: a review. Energy Educ Sci Technol 19:69–86

Hema M, Arivoli S (2007) Comparative study on the adsorption kinetics and thermodynamics of dyes onto acid activated low cost carbon. Int J Phys Sci 2:10–17

Ho YS, McKay G (1999) Pseudo-second order model for sorption processes. Process Biochem 34(5):451–465

Ibrahim MB, Sani S (2014) Comparative isotherms studies on adsorptive removal of Congo red from wastewater by watermelon rinds and neem-tree leaves. Open J Phys Chem 4:139–146

Ibrahim S, Fatimah I, Ang HM, Wang S (2010) Adsorption of anionic dyes in aqueous solution using chemically modified barley straw. Water Sci Technol 62:1177–1182

Interprofessional grouping of fruits (2015) Evolution of date production in Tunisia. http://gifruitscom/?page_id=2311&lang=fr Accessed 01 Feb 2018

Ip AWM, Barford JP, McKay G (2009) Reactive black dye adsorption/desorption onto different adsorbents: effect of salt, surface chemistry, pore size and surface area. J Colloid Interface Sci 337:32–38

Iqbal M, Schiewer S, Cameron R (2009) Mechanistic elucidation and evaluation of biosorption of metal ions by grapefruit peel using FTIR spectroscopy, kinetics and isotherms modeling, cations displacement and EDX analysis. J Chem Technol Biotechnol 84(10):1516–1526

Kesraoui A, Selmi T, Seffen M, Brouers F (2017) Influence of alternating current on the adsorption of indigo carmine. Environ Sci Pollut Res 24:9940–9950

Kilislioglu A, Bilgin B (2003) Thermodynamic and kinetic investigation of uranium adsorption on amberlite IR–118H resin. App Radiat Isot 50:155–160

Körbahti BK, Rauf MA (2008) Application of response surface analysis to the photolytic degradation of basic red 2 dye. Chem Eng J 138(1–3):166–171

Lagergren SK (1898) About the theory of so-called adsorption of soluble substances. Sven Vetenskapsakad Handingarl 24:1–39

Langmuir I (1918) The adsorption of gases on plane surfaces of glass, mica and platinum. J Am Chem Soc 40:1361–1403

Lee J, Ye L, Landen WO, Eitenmiller RR (2000) Optimization of an extraction procedure for the quantification of vitamin E in tomato and broccoli using response surface methodology. J Food Compos Anal 13:45–57

Limousy L, Ghouma I, Ouederni A, Jeguirim M (2017) Amoxicillin removal from aqueous solution using activated carbon prepared by chemical activation of olive stone. Environ Sci Pollut Res 24:9993–100004

Lodeiro P, Barriada JL, Herrero R, Sastre de Vicente ME (2006) The marine macroalga *Cystoseira baccata* as biosorbent for cadmium(II) and lead(II) removal: kinetic and equilibrium studies. Environ Pollut 142:264–273

Madrakian T, Haryani R, Ahmadi M, Afkhami A (2015) Spectrofluorometric determination of venlafaxine in biological samples after selective extraction on the superparamagnetic surface molecularly imprinted nanoparticles. Anal Methods 7(2):428–435

Mane V, Mall ID, Srivastava VC (2007) Kinetic and equilibrium isotherm studies for the adsorptive removal of brilliant green dye from aqueous solution by rice husk ash. J Environ Manag 84:390–400

Miraboutalebi SM, Nikouzad S, Peydayesh M, Allahgholi N, Vafajoo L, McKay G (2017) Methylene blue adsorption via maize silk powder: kinetic, equilibrium, thermodynamic studies and residual error analysis. Process Saf Environ Prot 106:191–202

Miyah Y, Lahrichi A, Idrissi M, Anis K, Kachkoul R, Idrissi N, Lairini S, Nenov V, Zerrouq F (2017) Removal of cationic dye "crystal violet"in aqueous solution by the local clay. J Mater Environ Sci 8(10):3570–3582

Mohamed M, Ouki S (2011) Removal mechanisms of toluene from aqueous solutions by chitin and chitosan. Ind Eng Chem Res 50:9557–9563

Mahmoudi K, Hosni K, Hamdi N, Srasra E (2015) Kinetics and equilibrium studies on removal of methylene blue and methyl orange by adsorption onto activated carbon prepared from date pits-A comparative study. Korean J Chem Eng 32(2):274–283

Mohanty K, Naidu JT, Meikap BC, Biswas MN (2006) Removal of crystal violet from wastewater by activated carbons prepared from rice husk. Ind Eng Chem Res 45(14):5165–5171

Muruganaadham M, Swaminathan M (2004) Solar photocatalytic degradation of a reactive azo dye in TiO2-suspension. Sol Energy Mater Sol Cells 81:439–457

Muthanna JA (2016) Preparation of activated carbons from date (Phoenix dactylifera L.) palm stones and application for wastewater treatments: review. Process Saf Environ Prot 102:168–182

Myers RH, Montgomery DC (2001) Montgomery response surface methodology. Wiley, 2nd edn

Pandey KK, Pitman AJ (2003) FTIR studies of the changes in wood chemistry following decay by brown-rot and white-rot fungi. Int Biodeterior Biodegrad 5:151–160

Ramteke LP, Gogate PR (2016) Removal of copper and hexavalent chromium using immobilized modified sludge biomass based adsorbent. Clean Soil Air Water 44:1051–1065

Raval NP, Shah PU, Shah NK (2016) Adsorptive amputation of hazardous azo dye Congo red from wastewater: a critical review. Environ Sci Pollut Res 23:14810–14853

Ravikumar K, Pakshirajan K, Swaminathan T, Balu K (2005) Optimization of batch process parameters using response surface methodology for dye removal by a novel adsorbent. Chem Eng J 105:131–138

Rozumová L, Životský O, Seidlerová J, Motyka O, Šafařík I, Šafaříková M (2016) Magnetically modified peanut husks as an effective sorbent of heavy metals. J Environ Chem Eng 4:549–555

Saeed A, Sharif M, Iqbal M (2010) Application potential of grapefruit peel as dye sorbent: kinetics, equilibrium and mechanism of crystal violet adsorption. J Hazard Mater 179:564–572

Saleh TA (2015) Isotherm, kinetic, and thermodynamic studies on Hg(II) adsorption from aqueous solution by silica- multiwall carbon nanotubes. Environ Sci Pollut Res 22:16721–16731

Samaka IS (2014) Removal of basic red 2 from industrial effluents using natural Iraqi material. Civil Environ Res 6:138–148

Samarghandi M, Hadi M, Moayedi S, Barjasteh Askari F (2009) Two-parameter isotherms of methyl orange sorption by pinecine derived activated carbon. Iranian J Environ Health Sci Eng 6:285–294

Sampranpiboon P, Charnkeitkong P, Feng X (2014) Equilibrium isotherm models for adsorption of zinc (II) ion from aqueous solution on pulp waste. WSEAS Trans Environ Dev 10:35–47

Santhi T, Manonmani S, Smitha T (2010) Kinetics and isotherm studies on cationic dyes adsorption onto annonasqumosa seed activated carbon. Int J Eng Sci 2:287–295

Shahbeig H, Bagheri N, Ali Ghorbanian S, Hallajisani A (2013) A new adsorption isotherm model of aqueous solutions on granular activated carbon. World J Modell Simul 9:243–254

Singh KP, Singh A, Singh U, Verma P (2012a) Optimizing removal of ibuprofen from water by magnetic nanocomposite using Box-Behnken design. Environ Sci Pollut Res 19:724–738

Singh KP, Rai P, Pandey P, Sinha S (2012b) Modeling and optimization of trihalomethanes formation potential of surface water (a drinking water source) using Box-Behnken design. Environ Sci Pollut Res Int 19:113–127

Solanki AB, Parikh J, Parikh RH (2007) Formulation and optimization of piroxicam proniosomes by 3-factor, 3-level Box–Behnken design. AAPS PharmSciTech 8:43–49

Subramani SE, Thinakaran N (2017) Isotherm, kinetic and thermodynamic studies on the adsorption behavior of textile dyes onto chitosan. Process Saf Environ Prot 106:1–10

Subramaniam R, Ponnusamy SK (2015) Novel adsorbent from agricultural waste (cashew NUT shell) for methylene blue dye removal: optimization by response surface methodology. Water Res Ind 11:64–70

Tempkin M, Pyzhev V (1940) Kinetics of ammonia synthesis on promoted iron catalyst. Acta Physiochim 12:327–356

Vijayaraghavan K, Padmesh TVN, Palanivelu K, Velan M (2006) Biosorption of nickel(II) ions onto Sargassum wightii: application of twoparameter and three- parameter isotherm models. J Hazard Mater 133:304–308

Wang L (2013) Removal of disperse red dye by bamboo-based activated carbon: optimisation, kinetics and equilibrium. Environ Sci Pollut Res 20:4635–4646

Weber W, Morris J (1963) Kinetics of adsorption on carbon from solution. J Sani Eng 89:31–60

Webi TW, Chakravort RK (1974) Pore and solid diffusion models for fixed-bed adsorbers. AICHE J 20:228–238

Yetilmezsoy K, Saral A (2007) Stochastic modeling approaches based on neural network and linear–nonlinear regression techniques for the determination of single droplet collection efficiency of countercurrent spray towers. Environ Model Assess 12:13–26

Zhu M, Yao J, Wang W, Yin XQ, Chen W, Wu X (2016) Using response surface methodology to evaluate electrocoagulation in the pretreatment of produced water from polymer-flooding well of Dagang Oilfield with bipolar aluminum electrodes. Desalin Water Treat 57:15314–15325